Crystallization of amorphous GeTe simulated by neural network potential addressing medium-range order

Supplementary Information

1. Details on the training data

The training data consist of various configurations as compiled in Table S1 with the number of training points and the sampling interval. In detail, the label 'Crystal' includes the hexagonal and fcc phases with strain, point defects such as self-interstitial, self-substitutional, and vacancy, or local vibrations at 700 K. In the case of the strained crystal, hydrostatic, volume-conserved uniaxial, and shear strain are considered, of which maximum strain of 5 % is applied to each axis. The label 'Liquid' and 'Quenching' indicate MD trajectories at 1000 K and quenched down to 300 K with a cooling rate of −15 K/ps, respectively. The melt-quench protocol is identical as described in Ref. [1]. The amorphous structure is obtained from the melt-quench method and its annealing MD at 500 K is labeled as 'Amorphous.' Heating of fcc GeTe is carried out at 1000 K for 5 ps, iterated until complete melting with an incremental temperature of 100 K. Transition from solid to liquid occurs at 1500 K, and the trajectories near the transition temperature is collected and labeled as 'Melting.' The shortest sampling interval of 20 fs is used at the moment of phase transition, compensating lack of the data stemming from its transient nature. 'Liquid (Ge or Te)' indicates the unary liquid phases at 1000 K, and interfaces are made between them to mix at 1500 K, labeled as 'Mixing liquid.' The label "Ring relaxation" consists of the DFT-relaxed trajectories of the amorphous structures obtained by c-NNP. The next subsections provide additional explanations for constructing the training set.

Table S1. Detailed information of the training data. In the amorphous, mixing liquid, melting, ring relaxation, multiple trajectories are used for sampling (2, 2, 2, and 5, respectively.) The temperatures for MD simulations are shown in parentheses.

Structure type	Number of atoms in a structure	Number of structures	MD time (ps)	Interval (fs)	Number of training points	$RMSE_{energy}$ (meV/atom)		$RMSE_{force}$ (eV/ Å)	
						c-NNP	m-NNP	c-NNP	m-NNP
Crystal									
(HEX)	6	102							
MD (700 K)	108	125	15	120					
(FCC)	8	61							
MD (700 K)	64	125	15	120	28,471	3.14	2.48	0.16	0.17
(Interstitials)	65	61							
(Substitutions)	64	16							
(Vacancies)	63	14							
Liquid (1000 K)	96	500	30	60	48,000	4.41	4.05	0.26	0.28
Amorphous (500 K)	96	251	5	40	24,096	7.24	6.20	0.26	0.28
Quenching (1000→300 K)	96	518	47	90	49,728	5.81	3.67	0.25	0.27
Melting (FCC→liquid)	96	352	5	100	33,792	5.11	3.47	0.23	0.26
(1400, 1500 K)			2.5	20					
Mixing liquid (Ge+Te)	160	240	12	50	57,920	3.75	3.07	0.26	0.30
(1500 K)	320	61	8	50					
Liquid (Ge or Te) (1000 K)	100	125	10	80	37,500	3.92	3.48	0.26	0.27
		250	10	40					
Ring relaxation (NNP→DFT)	96	774			74,304		3.54		0.16

1.1 Melting of fcc crystal

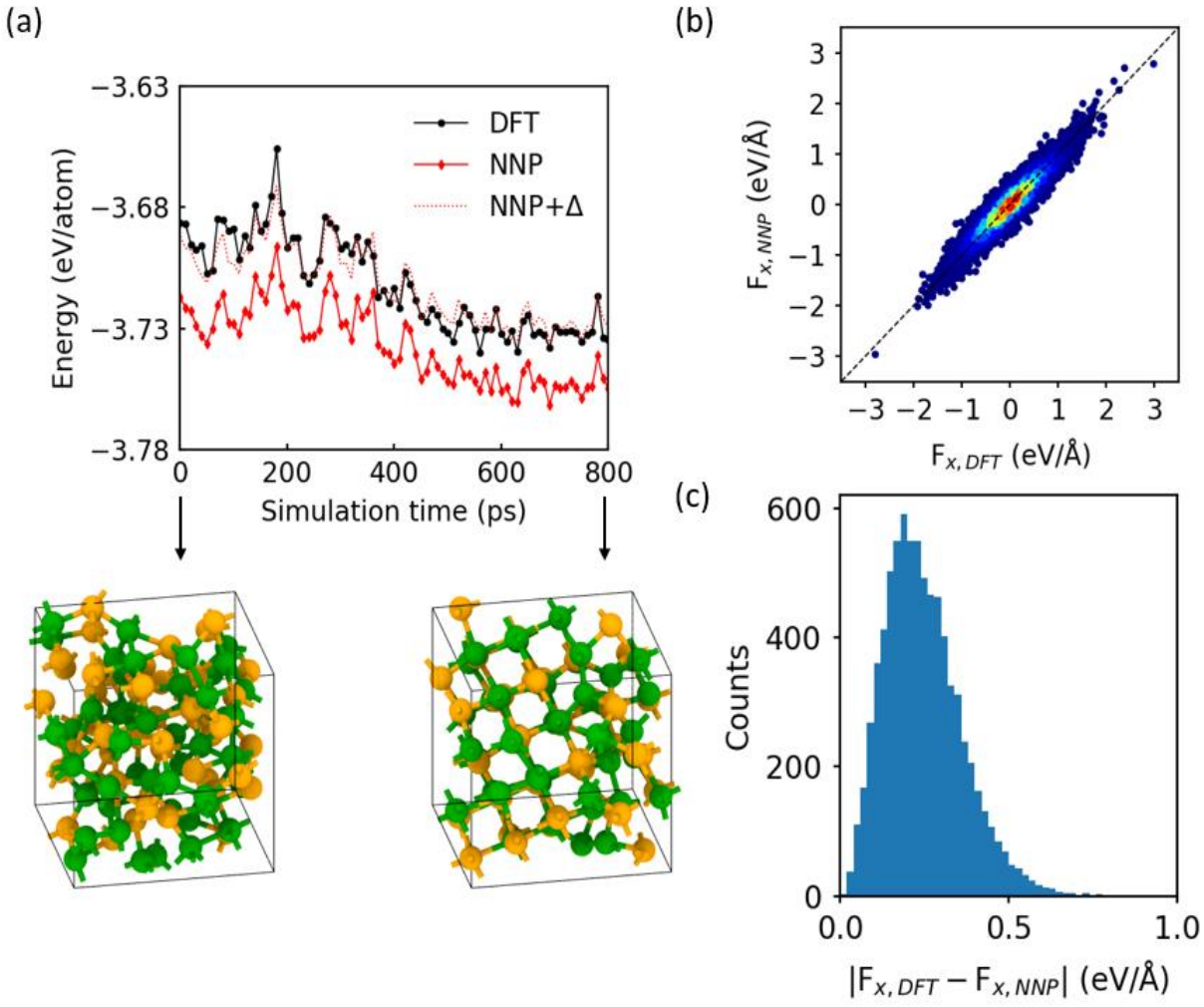

Fig. S1. (a) Evolution in time of energies calculated by DFT and m-NNP. The constant energy shift (Δ) of ~25 meV/atom is observed, but the relative potential energy surfaces are close to each other. The amorphous structure is not fully crystallized after 800 ps due to orientational mismatch. (b) The distribution of atomic force components in one direction. (c) Histogram of the magnitude of atomic force difference between DFT and m-NNP.

One might doubt that NNP has the ability to run crystallization simulation since the crystallization trajectory is not explicitly included in the training data. We found that the melting of fcc crystal data are the learnable points of crystallization data [2], as validations are followed about crystallization simulations: Using m-NNP, the 96-atom amorphous structures are generated

by the melt-quench method and crystallization simulations are performed at 600 K for 2 ns. Fig. S1(a) compares the potential energy surface along the crystallization process, and (b) and (c) show the force errors between DFT and NNP. Although RMSE for energy is 25 meV/atom, the relative potential energy surface is close to DFT. In addition, RMSE for force is 0.27 eV/Å, similar to that of amorphous structures in the validation set. Overall, the crystallization process simulated by m-NNP is in good agreement with DFT.

1.3 Mixing of unary Ge and Te liquid

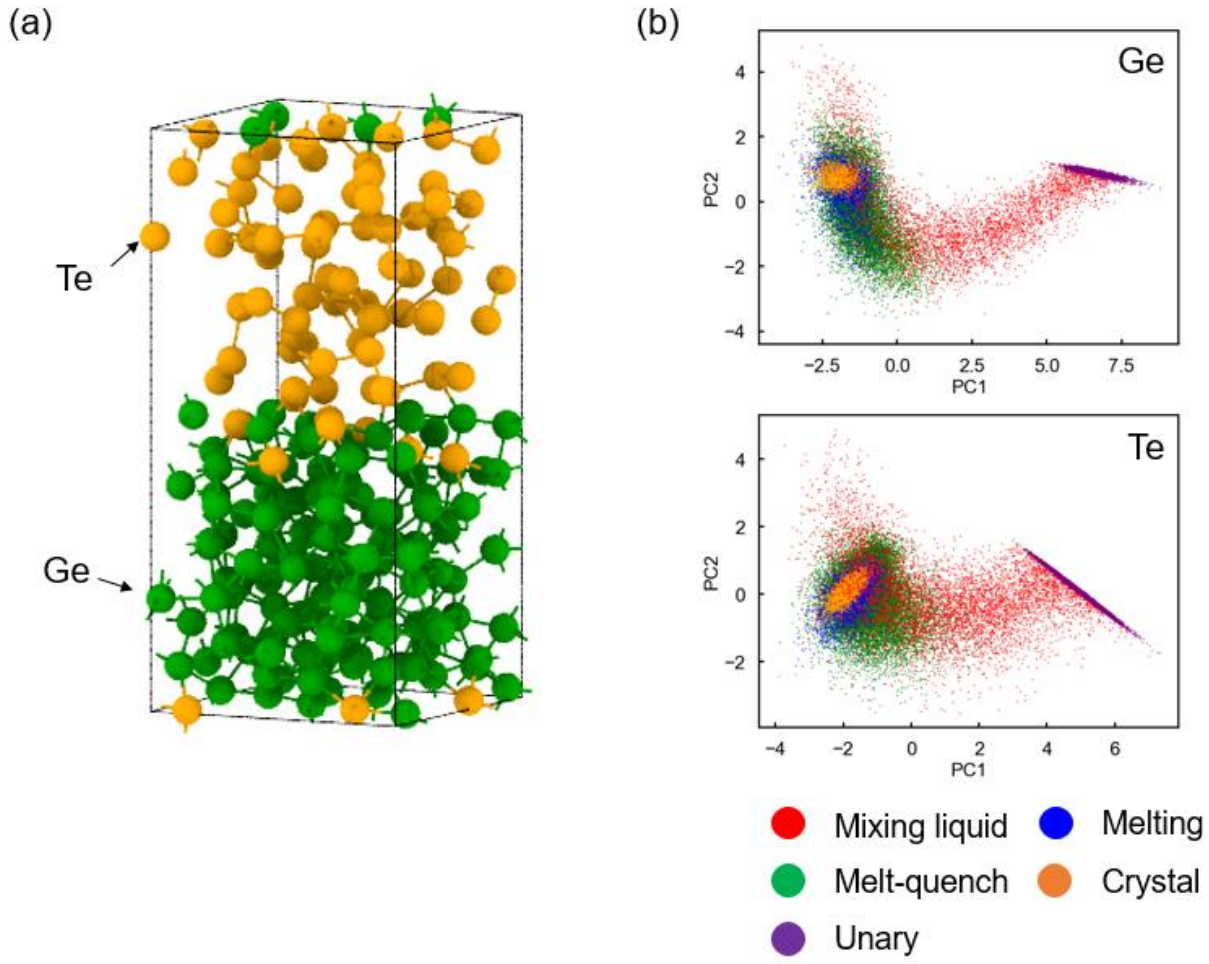

Fig. S2. (a) Ge-Te interface modeling comprised of the two unaries liquid slabs. (b) Principal component analysis (PCA) for the training data.

We found that liquid simulations of GeTe at 1000 K often induce phase separation into unary Ge and Te when the training set consists of only 1:1 composition. It is due to ad hoc energy mapping in the multi-component system [2], which results in the instability of NNP. To overcome this problem, data points should be close enough to each other. Therefore, we generate an interface model between unary liquid slabs as presented in Fig. S2(a), and heating at 1500 K until they mix to be liquid GeTe. In order to examine the distribution of training points in reduced dimensions, we carry out the principal component analysis (PCA). Figure S2(b) shows a distribution of the training set along directions of large variance by projecting data on the first (PC1) and second principal components (PC2), with distinct color for each subset. (The number is assigned by the descending order in variances.) It is seen that unary (purple) and binary (green) liquid data are connected via the mixing data (red). The data connection contributes to reliable atomic energy mapping, which increases the stability of NNP and prevents unphysical phase separations.

2. Learning curves

We take a two-step scheme to train NNP by manipulating energy and force coefficient of the loss function and learning rates with the definition in Ref. [3]. The energy coefficient is equal to 1.0 in both steps, while the force coefficient is set to be 1.0 in the first step and zero in the second step. We use learning rates of 10-2 and 10-5 for force and energy training, respectively. The Adam optimizer is used for both training steps with a batch size of 20. Figure S3 provides evolution of RMSE of energy and force as training proceeds. As a result, total force and energy RMSE is under 0.3 eV/Å and 5 meV/atom for both c-NNP and m-NNP, respectively.

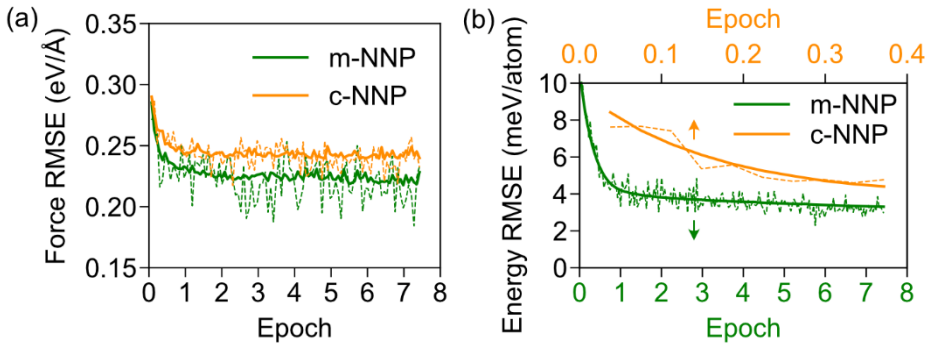

Fig. S3. Learning curves of (a) force training and (b) energy training. The solid lines and dashed lines indicate the RMSEs of the validation and training data, respectively.

We performed tests to determine the L2 regularization coefficient. As shown in Fig. S4, it appears that regularization effects are negligible on the overall learning curves since RMSEs for energy are below 10 meV/atom and differences between training (solid lines) and validation (dotted lines) errors are very small. However, large coefficients over 10-6 lead to under-training for the ring relaxation. That is to say, NNP prefers planar fourfold rings even after training the ring relaxation data. Although the L2 regularization coefficients below 10-8 lead to similar validation errors and energy correlation between DFT and NNP, we used L2 regularization coefficient of 10-8 to prevent unexpected overfitting.

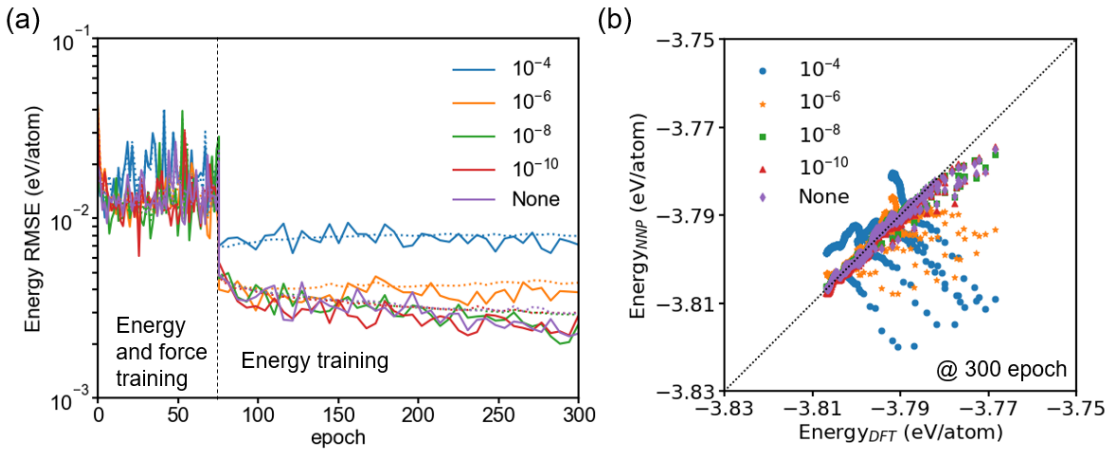

Fig. S4. With different regularization coefficients, (a) learning curves of RMSE for energy and (b) energy correlations between DFT and NNP after training of 300 epochs. The solid lines and dashed lines indicate the RMSEs of the training and validation data, respectively.

To examine variations in RMSE with respect to different initial weight distributions, we train two additional c-NNPs independently with the same training data (c-NNP2 and c-NNP3) The validation errors of energy are summarized in the Table S2. Discrepancies of a few meV/atom among subsets are often observed. The “amorphous” subset in c-NNP has the largest validation error, while the “quenching” has the largest one in c-NNP3. This reflects a stochastic nature of training errors and such fluctuations of validation errors among c-NNPs may result from initial weights of neural networks and choice of validation set. To add, when we increase the amorphous subset to encompass 120,000 data points, the validation error is still 4.55 meV/atom, which is similar to the values in Table S2. This may reflect that sufficient data points are provided in learning the amorphous state.

Table S2. Consistency of validation RMSEs of NNP training.

Structure type	$RMSE_{energy}$ (meV/atom)			$RMSE_{force}$ (eV/Å)		
	c-NNP	c-NNP2	c-NNP3	c-NNP	c-NNP2	c-NNP3
Crystal (700 K)	3.14	4.66	3.12	0.16	0.18	0.14
Liquid (1000 K)	4.41	5.08	4.74	0.26	0.27	0.27
Amorphous (500 K)	7.24	5.00	4.25	0.26	0.24	0.25
Quenching (1000→300 K)	5.81	5.68	7.26	0.25	0.25	0.25
Melting (FCC→liquid) (1400, 1500 K)	5.11	5.08	6.70	0.23	0.23	0.24
Mixing liquid (Ge+Te) (1500 K)	3.75	4.58	3.95	0.26	0.29	0.29
Liquid (Ge or Te) (1000 K)	3.92	4.28	4.50	0.26	0.27	0.26
Total	4.99	4.96	5.19	0.24	0.26	0.25

3. Structural properties of c-NNP

RDF and ADF of the liquid and amorphous structure are summarized in Fig. S5, including our work of DFT and c-NNP as well as previous NNP-based simulations [4]. It is noteworthy that density and the liquid temperature are slightly different between Ref. [4] and our work, where they are 31.6 atoms/nm^3 and 1150 K respectively while we use 34.6 atoms/nm^3 and 1000 K. Total RDF of liquid and amorphous structures is in good agreements among them.

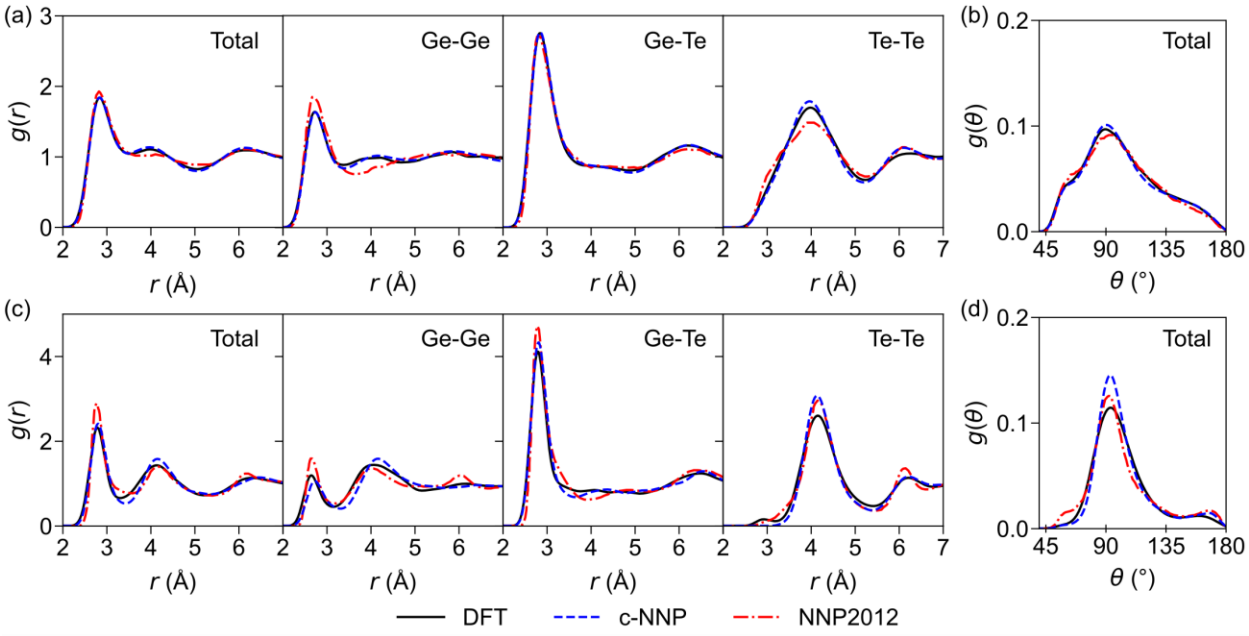

Fig. S5. (a) Total and partial RDF of liquid GeTe. (b) Total ADF of liquid GeTe. (c) Total and partial RDF of amorphous GeTe. (d) Total ADF of amorphous GeTe. The temperature of liquid and amorphous is 1000 K and 300 K respectively in our simulation and 1150 K and 300 K in the previous study 'NNP2012' [4]. The data is reconstructed from the reference, with renormalization of ADF.

4. Planarity of fourfold rings at the simulation conditions

We found that the incubation time is increased by reducing the number of the planar

fourfold rings in the amorphous state. Since the structural analysis was performed at 300 K (under glass transition temperature), the same analysis is performed at 500 K (above the glass transition temperature) and the results are shown in Fig. S6. The planar fourfold rings are more favorable in c-NNP than m-NNP in both densities and is more at the higher density (ρ_{crystal}) than the lower density (ρ_{device}). The structural features at 500K are consistent with those at 300K.

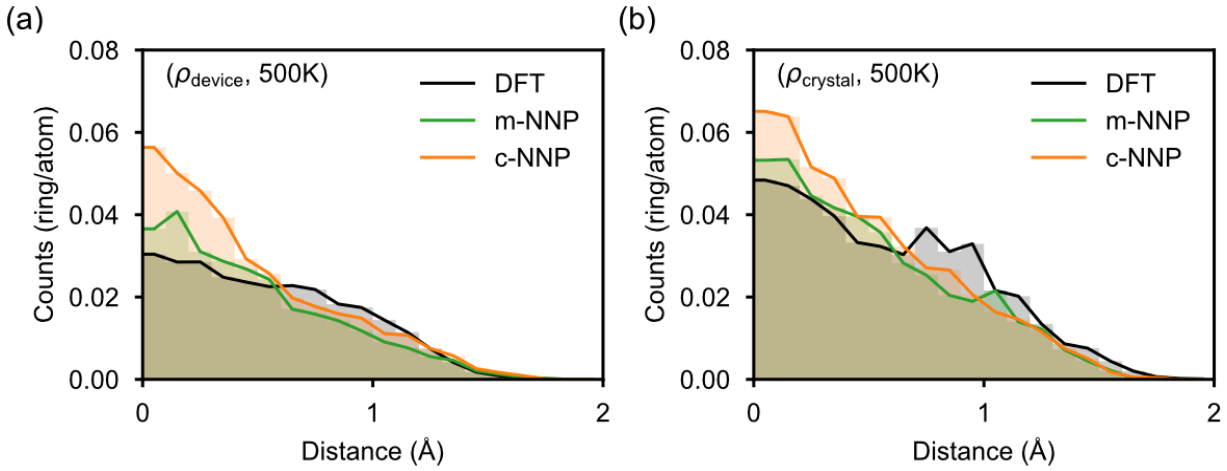

Fig. S6. Planarity of fourfold rings in a-GeTe at 500 K by DFT, m-NNP and c-NNP obtained by the same method as in Fig. 2(a) at (a) the device-condition and (b) crystalline density.

References

[1] D. Lee, G. Kang, K. Lee, S. Yoon, J. Kim, S. Han, First-principles calculations on effects of Al and Ga dopants on atomic and electronic structures of amorphous $Ge_2Sb_2Te_5$, J. Appl. Phys. 125 (2019) 035701.

[2] D. Yoo, K. Lee, W. Jeong, D. Lee, S. Watanabe, S. Han, Atomic energy mapping of neural network potential, Phys. Rev. Mater. 3 (2019) 093802.

[3] K. Lee, D. Yoo, W. Jeong, S. Han, SIMPLE-NN: An efficient package for training and executing neural-network interatomic potentials, Comput. Phys. Commun. 242 (2019) 95–103. (https://github.com/MDIL-SNU/SIMPLE-NN)

[4] G.C. Sosso, G. Miceli, S. Caravati, J. Behler, M. Bernasconi, Neural network interatomic potential for the phase change material GeTe, Phys. Rev. B 85 (2012) 174103.